Bonded PT Slab-Column Connections with and without Drop Panel Subjected to Earthquake Loading

U. Prawatwong
Suranaree University of Technology, Thailand

P. Warnitchai & C.H. Tandian
Asian Institute of Technology, Thailand

SUMMARY:
Results of tests to failure on two 3/5-scale models of bonded post-tensioned interior slab-column connections, without and with drop panel, are presented. The study's goals were to: (1) develop information on the seismic performance of typical bonded post-tensioned interior slab-column connections; and (2) investigate the effect of adding drop panel to improve the seismic performance of the interior connections. A lateral quasi-static cyclic loading routine, simulating earthquake actions, was applied to the models' top columns. Relevant design equations suggested by ACI 318-08 Building Code provisions for preventing stress-induced and deformation-induced failures as well as previous similar tests by others were compared with test results. We found that the presence of a drop panel effectively and significantly enhances the poor performance of the typical bonded post-tensioned interior connections. Our study indicates that the existing ACI 318-08 recommendation can be used for designing the bonded post-tensioned interior connections.

Keywords: slab-column connections, drop panel, post-tensioning (PT), punching shear, bonded tendons

1. INTRODUCTION

The use of post-tensioned slabs for building structural systems has become increasingly popular around the globe, but little research has been conducted on the seismic performance of bonded post-tensioned slab-column connections. It is widely known that slab-column connections are the most critical regions in a flat plate system. Under a strong earthquake ground motion, sudden and brittle punching failure may occur at a slab-column connection region due to a combination of direct gravity shear and eccentric shear from excessive earthquake-induced unbalanced moment between slab and column. In addition, extensive cracks in the connection region caused by repeated reversals of large lateral deformation may significantly deteriorate the shear strength of the connection. The punching shear failure at one connection may, in turn, initiate a progressive collapse of the entire building structures as notoriously shown in literatures. Mitchell et al. (1986) pointed out that such failure is the primary mode of failure in collapses of many waffle-slab and solid-slab during the 1985 Mexico earthquake.

Although numerous experimental studies on the seismic performance of slab–column connections have been carried out over the past four decades, most of them focused on the seismic response of reinforced concrete (RC) flat plates. A limited number of studies investigated the seismic capacity of PT flat plates (Hawkins 1981, Foutch et al. 1990, Qaisrani 1993, Martinez–Cruzado et al. 1994, Kang and Wallace 2006, Gayed and Ghali 2006). All tested PT specimens were hitherto made to represent unbonded flat plate connections. Therefore, the seismic performance of bonded PT slab-column connections has never been examined. Few guidelines and little information are available to designers.

This paper deals with reversed-cyclic tests to failure on two three-fifth scale models of prototype bonded post-tensioned interior slab-column connections. The first specimen, named S1, was carefully designed and constructed to represent a typical PT slab-column connection with no drop panel designed in Thailand. The second specimen, named S2, was an improved design of S1 by adding a drop panel. Each specimen was subjected to a lateral quasi-static cyclic loading routine to investigate its seismic performance through the elastic and inelastic ranges and finally until failure. The results are compared with existing design equations suggested by ACI 318-08 Building Code provisions for preventing stress-induced and deformation-induced failures as well as previous similar tests by others.

2. DESCRIPTION OF TEST PROGRAM

2.1 Prototype Structure and Specimen Design

A prototype building, within the range of typical multistory construction in Thailand, was used to design the scaled down models. The prototype building was 200 mm slab thickness, 8400 mm spans in each direction, and 3000 mm story heights. The span/depth ratio was approximately 42, which is commonly used in practice for flat plate structures. Cross-sectional areas of the columns were designed with 400 x 800 mm. The span dimension (8400 mm) was selected so that slab boundaries and column center of the scaled down models match tie-down location of the strong floor in the Structural Engineering Laboratory at Asian Institute of Technology (AIT). The relation of the model to the prototype is shown in Fig. 2.1.

S1 and S2 were designed as 3/5-scale models of prototype interior slab-column connections. As each specimen was developed based on the assumption that inflection points in the interior connection under earthquake-type loading occur at slab mid-span and column mid-story, half the total height of an interior column above and below the slab and half of the slab spans between adjacent columns on all four sides were modeled. Pin connections were attached to the points of contra-flexure under lateral loading. This model of connection was designed to produce bending moment and shear of the slab comparable to the prototype in the vicinity of the column where the most damage was expected.

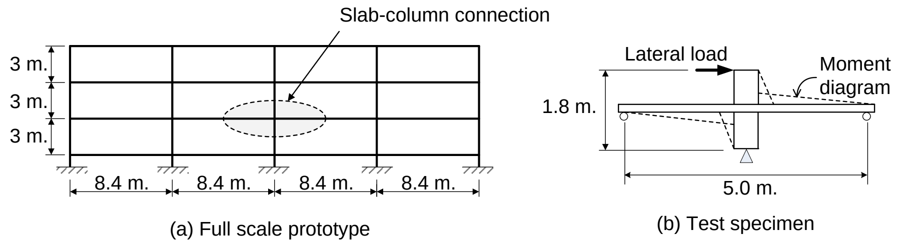

Figure 2.1. Relation of specimen to prototype structure

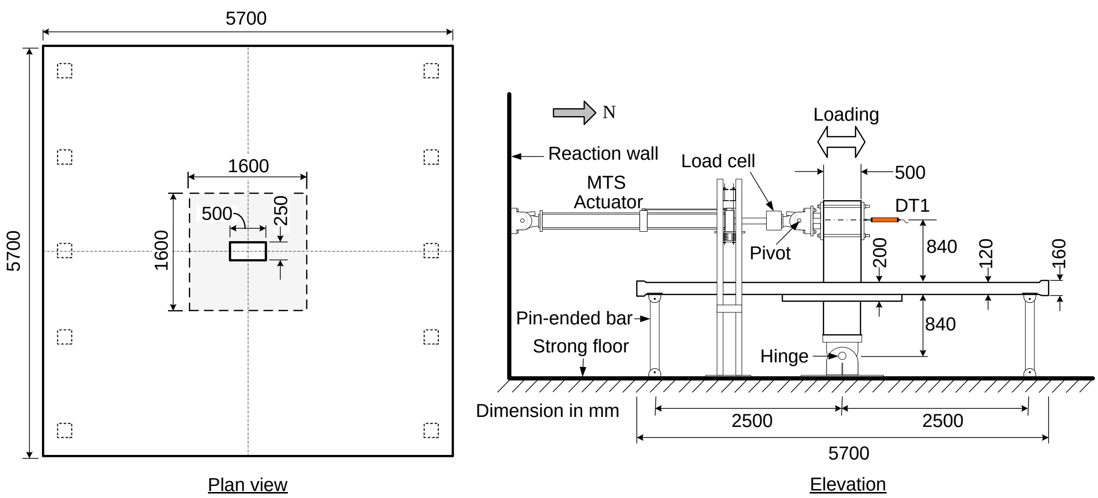

Figure 2.2. Interior slab–column connection specimen with drop panel and its dimensions

2.2 Description of Specimens

Each of the specimens in the series was identical in slab dimension, column dimension, tendon layout, and prestressing forces. The specimens were of normal weight concrete, 5700 mm square, 120 mm thick, and 250x500 mm column in the center of the panel (Fig. 2.2). The specimen S1 without drop panel, which was used as the control specimen, was modeled after typical connections found in most PT flat plate buildings in Thailand. On the other hand, the specimen S2 commonly followed the typical detail and loading of the specimen S1. The major variable for S2 was the additional drop panel. The additional drop panel in S2 was 1600 mm square and projected below the slab 80 mm. The supplementary reinforcing bars in S2 were provided and placed in such a way that the respective specimen may have better seismic performance than that of the specimen without drop panel. Fig. 2.3 and 2.4 show the reinforcement details of each of the specimens.

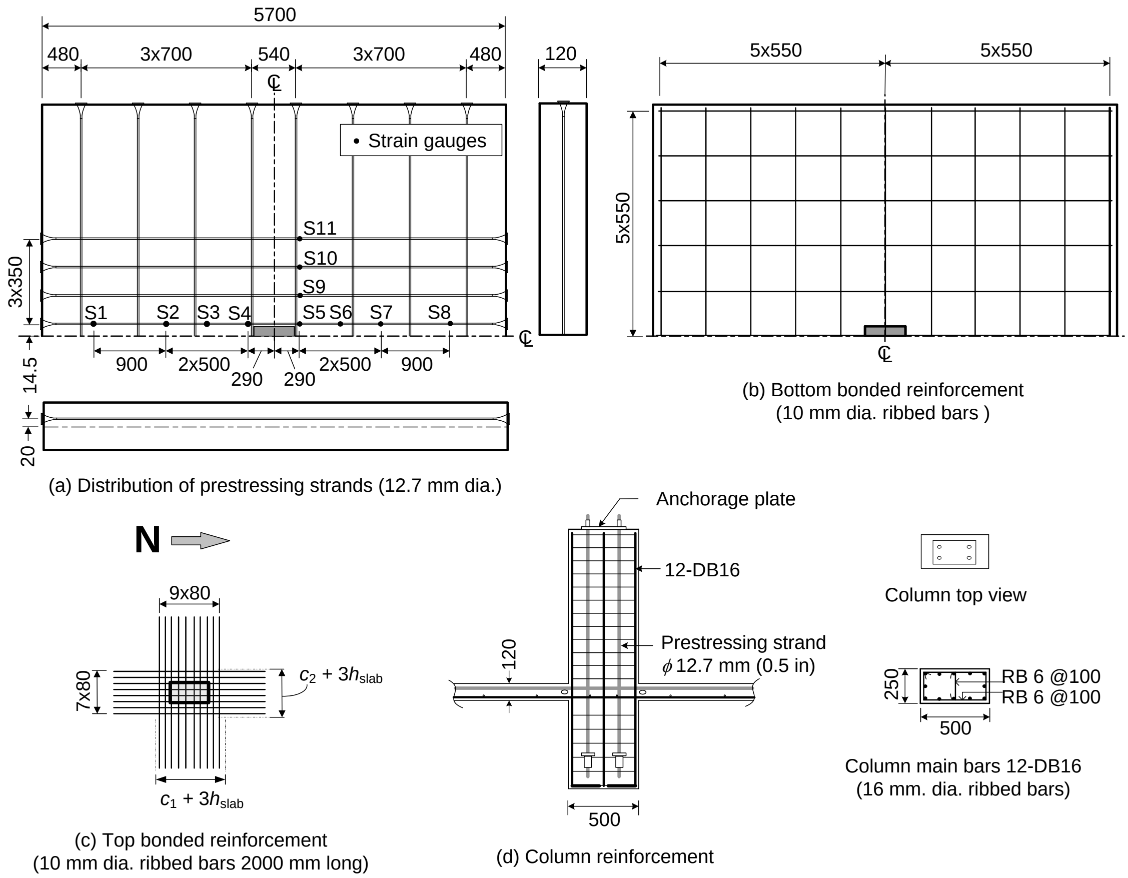

Figure 2.3. Reinforcement for Specimen S1 (dimension in mm)

The PT tendons in both models were ASTM A-416, Grade 270, 12.7 mm (1/2 in) diameter, seven-wire stress-relieved strands. Eight tendons were banded in the direction of loading (N-S direction) while the other eight tendons were uniformly distributed in the orthogonal direction (E-W direction). In each direction, there were no tendons passing through the column, similar to typical connections found in most PT flat plate buildings in Thailand. Each tendon was inserted into a flat (20 mm in height) galvanized duct to prevent bonding to the concrete before prestressing. To prevent damage due to high concentrations of stresses at the edges of the slab, an edge beam with sufficient reinforcing bars was provided on all sides of the slab. Distribution of prestressed tendons and their profile in slab of S1 and S2 are shown in Fig. 2.3a and 2.4a, respectively.

Supplementary reinforcement bars in peak negative moment in the vicinity of columns were provided in the slab of S1 as shown in Fig. 2.3c. The top reinforcements corresponded to a negative moment reinforcement ratio of 0.010 within an assumed effective width of $c+3h$ in each direction, where c is column dimension measured in the transverse direction of the top reinforcement, and h is the overall thickness of the slab. In addition, minimum areas of temperature and shrinkage reinforcement were provided in an orthogonal mesh as bottom reinforcement bars in the slab as shown in Fig. 2.3b. All bar arrangements were in such a way that the top and bottom bars in the direction of loading were placed at the outmost layer. A nominal clear concrete cover of 10 mm was specified for both top and bottom reinforcement.

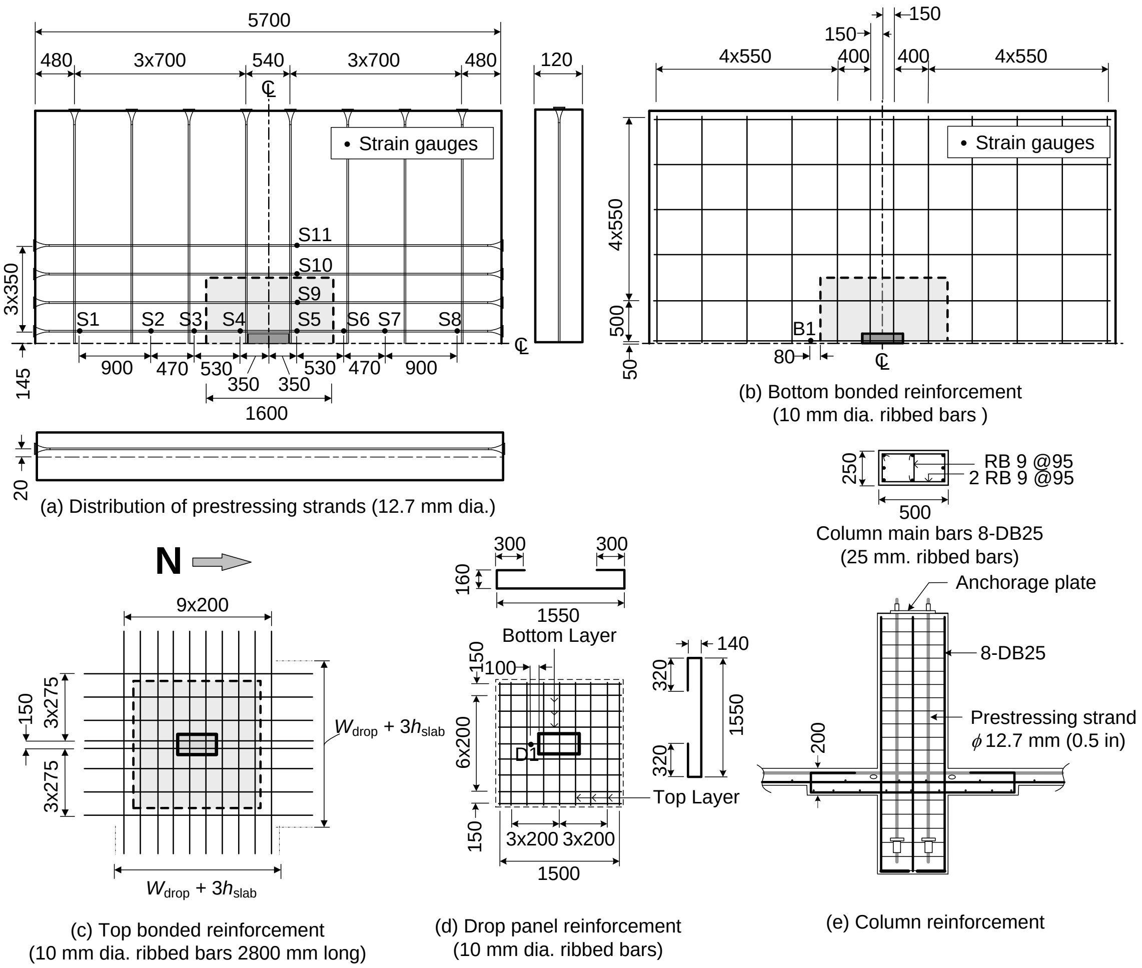

Figure 2.4. Reinforcement for Specimen S2 (dimension in mm)

The drop panel in S2 was reinforced with DB10 (10 mm diameter) deformed bars at the bottom face to counter tensile stresses caused by positive bending which might be induced by significant unbalanced moment due to lateral cyclic loading during the test. The reinforcement ratio of the drop panel, $\rho_{s,\ drop}$ = 0.003, was the same in each direction. To prevent anchorage failure of the bottom reinforcing bars in the drop panel, the vertical legs with development length of 40 times bar diameter were extended into the main slab. Fig. 2.4d shows the layout of the reinforcing bars within drop panel.

S2 also contained the supplementary top reinforcement bars at the top of its slab according to Section 18.9.3 of ACI 318-95 building code similar to those of S1. The supplementary top reinforcement bars, which were the same number of top bars as in S1, were distributed along an assumed effective support width of $W_{drop}+3h$ in the middle of the column in both directions (Fig. 2.4c), where W_{drop} is the width of the drop panel, and h is the total thickness of the slab outside the drop panel. The assumed effective support width was according to Section 13.1.2 of ACI 318-08 building code. The supplementary top reinforcement ratio within the drop panel corresponded roughly to 0.002 in each direction. The top bars were extended into the slab around the drop panel and cut off at a distance of 600 mm from the edge of the drop panel to provide development length as recommended in Section 21.7.5 of ACI 318-

08. In addition, two continuous bottom bars were placed over the column in each direction according to Section 18.12.7 and 13.3.8.5 of the code to prevent progressive collapse in the event of a connection shear failure.

In each of the specimens, sufficient transverse and longitudinal reinforcing bars were provided so the column would remain elastic without experiencing either flexural or shear failure during the test. In addition, vertical prestressing forces of 588 kN were applied to the column by four unbonded tendons to simulate the effects of gravity loads from the upper floors. The details of reinforcement for the columns in S1 and S2 are given in Fig. 2.3d and 2.4e, respectively.

Each of the specimens was cast with ready-mix concrete. The model slabs were prestressed with eight tendons in each direction when the concrete slab gained sufficient strength. An effective force of 147.2 kN, corresponding to a stress of 0.80 f_{pu}, was applied to each tendon to produce the average prestress levels shown in Table 2.1. After the tendons were prestressed and the end recesses were filled, all galvanized ducts were grouted to provide an effective bond between the tendons and the ducts.

Table 2.1. Summary of Parameters and Properties of Model Slabs

Property (1)	Slab S1 (2)	Slab S2 (3)
1. Thickness of slab, in mm	120	120
2. Drop panel size, in mm	None	1600 x 1600 x 80
3. Column height, in mm	1800	1800
4. Cross-sectional area near critical section, sq mm	6.84×10^5	8.12×10^5
5. Effective depth of strands, d_p, in mm		
N-S direction	80	160
E-W direction	60	140
6. Concrete strength, in MPa		
f_{ci}' at time of stressing	20.0 (4 days)	31.8 (6 days)
f_c' at time of testing	41.1 (43 days)	45.9 (43 days)
7. Steel strength of strands, in MPa		
f_{pu}, tensile strength	1902	1947
f_{py}, yield strength at 1% elongation	1780	1763
8. Steel strength of DB10, in MPa		
f_u, tensile strength	587	491
f_y, yield strength	503	324
9. Average compressive stress f_{pc}, in MPa		
P/A in N-S direction	1.72	1.45
P/A in E-W direction	1.72	1.45

2.3 Testing of Specimens

It is well known that a major parameter that influences the lateral displacement capacity of slab–column connections is the gravity shear ratio (V_g/V_0), where V_g is the direct gravity shear force acting on the slab critical section and V_0 is the slab punching strength in the absence of moment transfer as defined in ACI 318-08. The lateral displacement capacity and ductility generally drops as the magnitude of the connection gravity shear ratio (V_g/V_0) increases (Pan and Moehle 1989, Kang and Wallace 2006). Hence, S1 was loaded by a large number of sand bags on top and below the slab to simulate the gravity shear ratio (V_g/V_0) of 0.28, which is approximately the average value of those found in slab-column frame buildings in Thailand (Warnitchai et al. 2004). The same gravity loading was also applied to S2. But since the slab in the connection region was thicker due to the presence of drop panel, the gravity shear ratio of 0.13 was obtained for this case.

The seismic movement was simulated by applying lateral displacement at the top of the column through a MTS servo controlled hydraulic actuator as depicted in Fig. 2.2. The hydraulic actuator was mounted to a rigid reaction wall. A typical displacement–controlled reversed cyclic lateral loading test was carried out to both specimens with monotonically increasing target drifts of 0.25%, 0.50%, 0.75%, 1.00%, 1.25%, 1.50%, 2.00%, 2.50%, 3.00%, 4.00%, and so on… At each target drift, two complete cyclic displacement loops were conducted. The loading was terminated after the punching cone had formed completely. Note that the respective target drift is defined as the ratio of the lateral displacement of column at lateral loading point to the column height, which is 1.8 meter.

During the testing of both specimens, all measurement data were recorded at each loading step. A load cell and a displacement transducer were installed at top of the column (Fig. 2.2) to monitor detailed overall force-displacement relations of the connections throughout the loading history. The strain in some post-tensioning tendons and supplementary reinforcing steel were monitored by electrical resistance type strain gauges installed on the bars prior to casting the specimens on locations as shown in Fig. 2.3 and 2.4. Further details of instrumentation can be found in Pongpornsup (2003) and Tandian (2006).

3. EXPERIMENTAL RESULTS

3.1 Overall Response

Due to space limitation, only some results are presented in this paper. Fig. 3.1a and 3.1b give the lateral force-drift relations of S1 and S2, respectively. The figures show that both specimens displayed long and narrow hysteresis loops, demonstrating a limited ability to dissipate energy of bonded PT interior slab-column connections. As the drift level became higher, in general, specimen stiffness degraded more and the hysteresis loops were wider. No significant pinching was observed from the hysteresis loops of either specimen. Both S1 and S2 experienced punching failure. Punching failure in each of the specimens was characterized by a sudden drop of lateral load-carrying capacity to less than 50% of its maximum force attained during the tests.

S1, without a drop panel, could only withstand 2.0% drift (Fig. 3.1a). After the maximum lateral load of 107 kN was attained, this specimen suddenly failed in brittle punching shear and completely lost its lateral strength and stiffness while no peak load saturation was perceived in advance. It is likely that the higher gravity shear ratio in the first test was a key factor that caused early failure in punching shear in this specimen. S2 (with drop panel) attained 80% higher lateral load-carrying capacity than the control specimen (S1). As can be seen in Fig. 3.1b, S2 exhibited a saturation of peak load for a drift of 2% to 6%, indicating that flexural yielding took place long before punching failure. Until the end of the test, the specimen with the additional drop panel showed much higher drift capacity at about 6% at punching failure than the one without the drop panel.

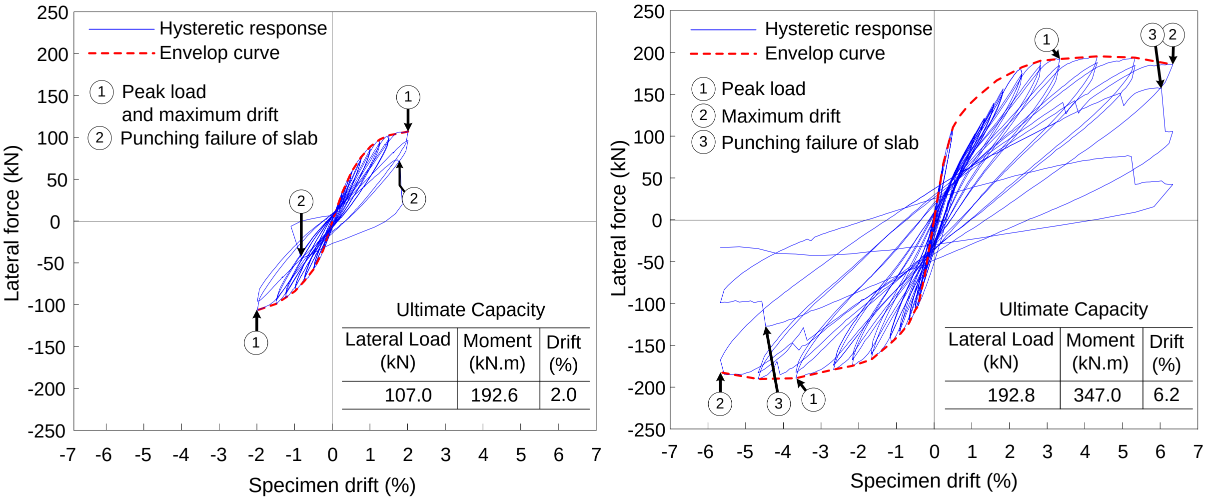

(a) Specimen without drop panel

(b) Specimen with drop panel

Figure 3.1. Lateral force-drift results

3.2 Comparison of Shear Stresses

In the following, the ACI model for the design of slab-column connections as shown in Fig. 3.2 is used to calculate the eccentric shear stress due to a gravity shear V_u and an unbalanced moment M_u along the critical section at $d/2$ from the column face. For the specimen with drop panel (S2), two critical sections as shown in Fig. 3.2a must be investigated, where d_1 is the average effective depth of the slab within thickened drop panel region and d_2 is the average effective depth of the slab outside drop panel.

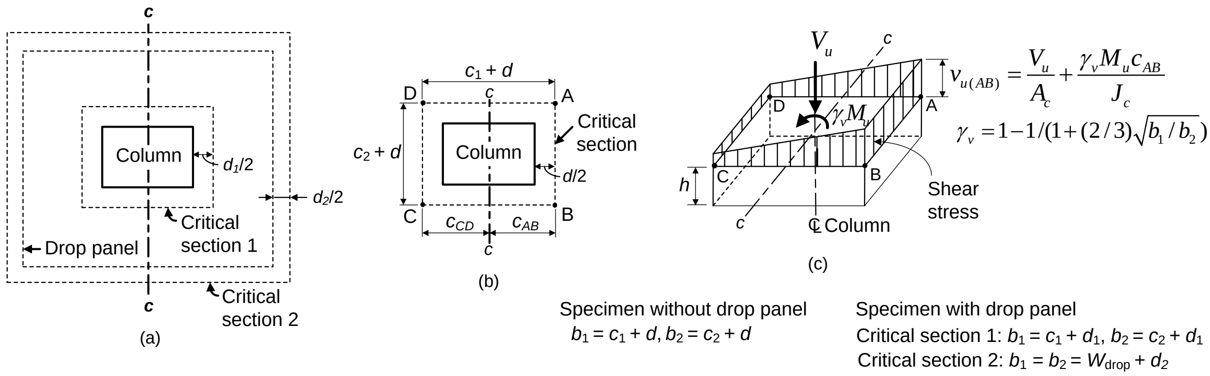

Figure 3.2. Critical sections at interior column for linear varying shear stress according to ACI Building Code (a) slab with drop panel; (b) slab without drop panel; (c) stress distribution along critical section.

The maximum shear stresses at the critical sections are expressed by the well-known equation shown below.

$$v_{u(AB)} = \frac{V_u}{A_c} + \frac{\gamma_v M_u c_{AB}}{J_c} \tag{3.1}$$

where $A_c = b_0 d$; $b_0 = 2(b_1 + b_2)$ = perimeter of critical section for shear in slab; d is the effective depth of the slab; c_{AB} is the distance from the centroidal axis of the critical section to line AB (Fig. 3.2b); J_c is a property of the critical perimeter analogous to the polar moment of inertia; and γ_v is the fraction of the unbalanced moment transferred by eccentricity of shear stress and is given in Fig. 3.2c.

Eqn. 3.1 shows that the maximum stress is the sum of uniformly distributed gravity shear and non-uniform lateral-force-induced shear. The gravity shear V_u in each specimen is computed from a linear finite analysis, which may have some estimated error, but the error is not so important since the gravity shear stress is low when compared with the lateral-force-induced shear (Table 3.1). The lateral-force-induced (or moment-induced) shear is estimated from $\gamma_v M_u$. For each specimen, the unbalanced moment M_u can be accurately determined by multiplying the peak lateral force by the column height (1800 mm) of the specimen. Based on the peak unbalanced moment (M_u) and the gravity load (V_u) on the test specimens, the maximum shear stresses according to the ACI model for S1 and S2 were obtained and listed in Columns 7 of Table 3.1.

Table 3.1. Ultimate Shear Stresses [a]

Specimen (1)	V_u (kN) (2)	M_u (kN.m) (3)	γ_v (4)	Shear stress, v_u (MPa): From direct shear (5)	From moment transfer (6)	Total (7)	$v_u / \sqrt{f_c'}$ (8)
S1	118	192.6	0.467	0.65	2.86	3.51	0.55
S2 (Inner section)	120	347.0	0.458	0.35	2.35	2.70	0.40
S2 (Outer section)	120	347.0	0.400	0.18	0.38	0.56	0.08

Notes: [a] No load factors were used in calculations.

To apply Eqn. 3.1 to PT slab-column connections, however, some value must be assumed for the effective depth d. It is appropriate to take d as the greater of two values, the actual effective depth (d) or $0.80h$, in accordance with the concepts of ACI 318-02. For PT slabs in both specimens, all effective depths were less than $0.8h$ and therefore the latter value ($0.8h$) was used.

In Fig. 3.3a, the maximum shear stresses v_u of S1 and S2 in Table 3.1 are plotted and compared with shear stress limits expressed by Eqn. 11-34 of ACI 318-08 and by previous works from other investigators. The test data from previous works, represented by the black dots, were summarized by ACI-ASCE Committee 423 (1974). They were mostly obtained from tests conducted for connections transferring shear only, and all tested PT specimens were unbonded flat plate connections that failed in shear. These test data show clearly that though the normalized shear stress at failure generally increases with the increase in f_{pc} as predicted by Eqn. 11-34 of ACI, the stress is significantly higher than the code-specified limit, indicating a built-in safety margin of the code equation. To determine the true stress limit, an empirical best-fit equation ($v_u = 0.46\,(f_c')^{1/2} + 0.32\,f_{pc}$) was derived from these test data as depicted in Fig. 3.3a. This best-fit equation therefore represents the most likely value of shear stress at failure in slab-column connections.

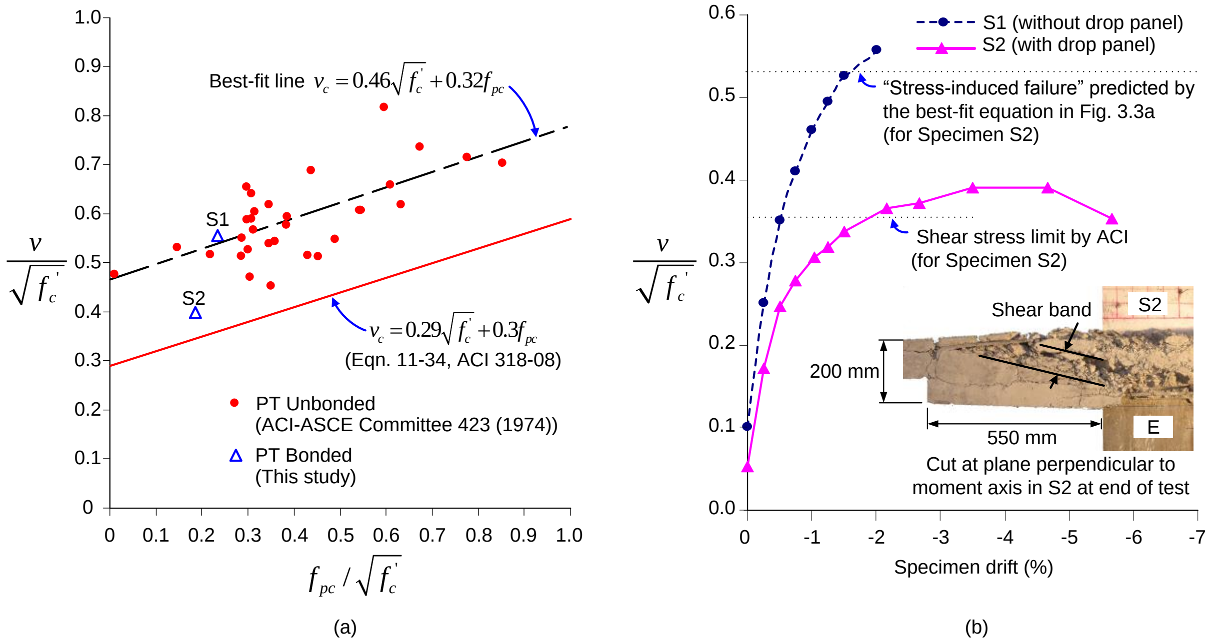

Figure 3.3. (a) Test data of Specimen S1 and S2 versus ACI 318-08 equation, (b) variation of maximum shear stress on critical section of the test specimens with specimen drift

Fig. 3.3a shows that the shear stresses at failure in S1 and S2 are both higher than the corresponding code-specified limits, suggesting that the code equation can be conservatively used for the design of bonded PT slab-column connections against stress-induced failure. For S1, where a sudden punching shear occurred at a low drift level while the stress was still increasing (Fig. 3.3b), the stress at failure is very close to the value predicted by the best-fit equation. The result of S1 therefore conforms well with those of available experimental data where failures belong to stress-induced type.

In S2, however, the stress at failure was higher than the code-specified limit but significantly lower than the value predicted by the best-fit equation. Moreover, the shear stress became 'saturated' at the drift level of around 2% (Fig. 3.3b), but the punching shear failure occurred much later at the drift level of 6%. S2 obviously showed ductile behaviour as opposed to the brittle behaviour found in S1. The punching shear failure at the high drift of 6% in S2 was believed to happen as a result of slab shear strength degradation by flexural cracks in the slab critical region. When the degraded shear strength dropped below the saturated shear stress, punching shear failure developed.

3.3 Comparison of Drift Capacity

For seismic design, ACI 318-08 provides guidance for the evaluation of shear reinforcement requirements at slab-column connections and design story drift limit, which is empirically bilinear as a function of gravity shear ratio. This limit is based primarily on tests of isolated, RC slab-column connections subjected to quasi-static loading.

Fig. 3.4 shows a plot of the gravity shear ratio and drift capacity at punching of both specimens from the current study, along with other test results of slab-column specimens without shear reinforcement. Most of the test results of RC slab-column specimens were collected and compiled by Pan and Moehle (1989), while those of unbonded PT slab-column interior connections were tested by Trongtham and Hawkins (1977) and Qaisrani (1993) and summarized by Kang and Wallace (2006). ACI 318-08 design drift limit for slab-column connections is also plotted in Fig. 3.4 for reference.

Contrary to the results of unbonded PT slab-column connections, where the drift capacity is more than twice ACI 318-08 drift limit in every case, the results of the two bonded PT slab-column connections do not show that they always possess higher drift capacity. Instead, the results are more or less consistent with those of RC specimens, suggesting that ACI 318-08 design drift limit could also be used for bonded PT slab-column connections.

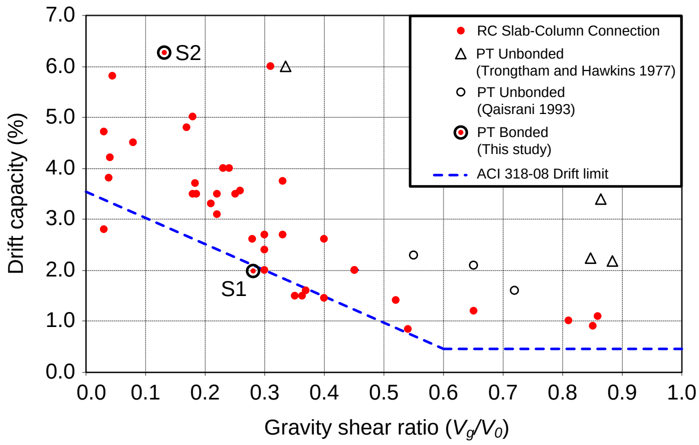

Figure 3.4. Gravity shear ratio versus drift capacity at punching for RC and PT slab-column connections

4. CONCLUSIONS

1. S1 showed non-ductile behavior under reversed cyclic loading. A sudden stress-induced punching shear failure developed at a low lateral drift level of 2%. The shear stress level at failure matched well with the average stress limit of unbonded PT slab-column connections, suggesting that the existing ACI's formula for stress limits can also be applied when designing bonded PT slab-column connections.

2. Adding a drop panel to a bonded PT slab-column connection effectively and significantly enhances its overall seismic performance. S2 exhibited dramatic increases in lateral strength and lateral deformation capacity compared to those of S1.

3. Ductile behavior in S2 was clearly demonstrated by its lateral force-drift relationship. This was evidently caused by flexural yielding in the slab, leading to shear stress saturation in the slab's critical region at a level below shear strength. Stress-induced failure was therefore inhibited. S2 finally failed by punching shear after a very high drift level of 6%, when the degraded shear strength dropped below the saturated shear stress. The results also suggest that ACI318-08's design drift limit could be used for bonded PT slab-column connections.

ACKNOWLEDGMENTS

This experimental work was conducted with funding provided by the Thailand Research Fund (TRF) and the Siam City Cement Public Company Limited (SCC). The prestressed strands, ducts, and anchors used in the tests were donated by the Concrete Products and Aggregate Company (CPAC) Limited. Heartfelt gratitude is conveyed to TRF, SCC, and CPAC for supporting this research program.

REFERENCES

ACI-ASCE Committee 423 (1974). Tentative Recommendations for Prestressed Concrete Flat Plates. *ACI Journal*. **67:2**, 61-71.

ACI Committee 318. (1995). Building Code Requirements for Structural Concrete (ACI 318-95) and Commentary. American Concrete Institute, Farmington Hills, US.

ACI Committee 318. (2002). Building Code Requirements for Structural Concrete (ACI 318-02) and Commentary. American Concrete Institute, Farmington Hills, US.

ACI Committee 318. (2008). Building Code Requirements for Structural Concrete (ACI 318-08) and Commentary. American Concrete Institute, Farmington Hills, US.

Foutch D.A., Gamble W.L. and Sunidja H. (1990). Tests of post–tensioned concrete slab–edge column connections. *ACI Structural Journal*. **87:2**, 167–179.

Gayed R.B. and Ghali A. (2006). Seismic–resistant joints of interior columns with prestressed slabs. *ACI Structural Journal*. **103:5**, 710–719.

Hawkins, N.M. (1981). Lateral load resistance of unbonded post–tensioned flat plate construction. *PCI Journal*. **26:1**, 94–116.

Kang, T.H.K. and Wallace, J.W. (2006). Punching of Reinforced and Post-Tensioned Concrete Slab-Column Connections. *ACI Structural Journal*, **103:4**, 531-540.

Martinez–Cruzado, J.A., Qaisrani, A.N. and Moehle, J.P. (1994). Post–tensioned flat plate slab–column connections subjected to earthquake loading. *Fifth U.S. National Conference on Earthquake Engineering*. **Vol II**: 139–148.

Mitchell, D., Adams, J., Devall, H.R., Lo, C.R. and Weichert D. (1986). Lessons from the 1985 Mexican earthquake. *Canadian Journal of Civil Engineering*. **13:5**, 535-557.

Pan, A. and Moehle, J.P. (1989). Lateral displacement ductility of reinforced concrete flat plates. *ACI Structural Journal*. **86:3**, 250-258.

Pongpornsup, S. (2003). Seismic Performance of Post-Tensioned Interior Flat Slab-Column Connections, Master Thesis no. ST 03-18, Asian Institute of Technology, Thailand.

Qaisrani, A.N. (1993). Interior Post-Tensioned Flat-Plate Connections Subjected to Vertical and Biaxial Lateral Loading, Doctoral Dissertation, Department of Civil Engineering, University of California-Berkeley, California, US.

Trongtham, N. and Hawkins, N.M. (1977). Moment Transfer to Columns in Unbonded Post-Tensioned Prestressed Concrete Slabs, Report SM77-3, Department of Civil Engineering, University of Washington-Seattle, Seattle, Washington, US.

Tandian, C.H. (2006). Seismic Performance of Bonded Post-Tensioned Interior Flat Slab-Column Connections with Drop Panel, Master Thesis no. ST 06-16, Asian Institute of Technology, Thailand.

Warnitchai, P., Pongpornsup S., Prawatwong U. and Pimanmas A. (2004). Seismic performance of post–tensioned interior flat slab–column connections. *Third International Symposium on New Technologies for Urban Safety of Mega Cities in Asia*. 147–156. Agra, India.